International Journal of Solids and Structures 46 (2009) 4169–4180

Contents lists available at ScienceDirect

International Journal of Solids and Structures

journal homepage: www.elsevier.com/locate/ijsolstr

On the deep penetration and plate perforation by rigid projectiles

Z. Rosenberg *, E. Dekel

RAFAEL, Balistics Center, P.O. Box 2250, Haifa, Israel

ARTICLE INFO

Article history:
Received 23 March 2009
Received in revised form 4 June 2009
Available online 11 August 2009

Keywords:
Penetration
Plate perforation
Rigid projectiles

ABSTRACT

We present results of a large number of 2D numerical simulations in which we investigated various aspects in the deep penetration of rigid short projectiles into semi-infinite targets, as well as their perforation through thin metallic plates. In particular, we analyze the effect of the entrance phase on the penetration characteristics of short ogive and spherical nosed projectiles. The second issue which we investigate here concerns the perforation of metallic plates by sharp nosed projectiles. Our simulation results show that a simple model, which is based on energy conservation, accounts for the residual velocities when the target is penetrated by the ductile hole enlargement process. In addition, we define a new concept, the effective resisting stress which the plate exerts on the projectile during perforation. We show that it has some valuable insights for the process of perforation and we perform a parametric study to understand its dependence on various parameters. This effective stress, which determines the ballistic limit velocity of the projectile, depends on the strength of the plate, as well as on its thickness, as we show here.

1. Introduction

In a recent paper (Rosenberg and Dekel, 2009) we analyzed the penetration process of rigid long rods, into semi-infinite targets, using 2D numerical simulations with the AUTODYN code. In particular, we followed the decelerations of rods with different nose shapes, as they penetrated various targets (aluminum, steel) with different yield strengths. One of the main conclusions of that work is that for each rod/target combination there exists a threshold impact velocity (V_c) below which the deceleration of the rod is constant throughout the whole penetration process. Moreover, this deceleration does not depend on impact velocity, as long as it is below V_c. From these constant declarations we obtained values for the resisting stress (R_t), which the target exerts on the rod, for several rod/target combinations, in terms of target strength and the nose shape of the rod. For impact velocities above V_c the deceleration of the rigid rod is velocity dependent and a dynamic term (target inertia) has to be added to R_t. In addition, we were able to construct simple formulas for the penetration depths of rigid rods at impact velocities below and above V_c. The predictions from these equations were found to agree with experimental data from the works of Forrestal and his colleagues (see Forrestal et al., 1991; Piekutowski et al., 1999 for example), for rigid steel rods penetrating various aluminum targets. One of the interesting observations, from those simulations, was that the constant deceleration which acts on the rod is reached at penetration depths of about 4–6 rod diameters. This is a clear indication for the effect of the entrance phase on the penetration process. In fact, the influence of the entrance phase was already manifested in the classical work of Bishop et al. (1945) who measured the force needed to push a conical-nosed steel rod into a thick copper plate. This force reached a constant value only after the rod penetrated a depth of about 4–5 rod diameters. These observations, of a constant resisting force at deep penetrations, are in contrast with the dynamic cavity expansion analysis of Goodier (1965) and we discuss this discrepancy here.

The numerical simulations described here are focused on two issues; the first is the penetration of rigid short projectiles into semi-infinite metallic targets, at impact velocities of 0–1.5 km/s (the so-called ordnance range). At these velocities the entrance phase plays a major role in the penetration process of short projectiles (with length to diameter ratios of $L/D = 3$–5). The second subject of the present work concerns the perforation of finite targets by sharp rigid projectiles (either short or long). The perforation process of relatively thin metallic plates is even more complex because of the back surface effects which reduce the resisting stresses on the projectile, in addition to the effects of the front face. Our simulations, for conical-nosed tungsten projectiles, follow the experimental results of Forrestal et al. (1990), in order to highlight several issues regarding perforation experiments, in terms of residual velocities and ballistic limit velocities.

2. Numerical simulations

The simulations were performed with the AUTODYN 2D code using the Lagrange processor for the rigid projectiles and the Euler

* Corresponding author.
E-mail addresses: zvirosenberg@yahoo.com, zvir@rafael.co.il (Z. Rosenberg).

0020-7683/$ - see front matter © 2009 Elsevier Ltd. All rights reserved.
doi:10.1016/j.ijsolstr.2009.07.027

processor for the targets. As in (Rosenberg and Dekel, 2009), the diameter of the projectiles is 6 mm and their strength 50 GPa (von-Mises yield criterion). This high strength ensures that the projectiles stay rigid at all impact velocities investigated here. The fact that projectiles can stay rigid even when they impact certain targets at velocities of 1.5 km/s is not surprising when one considers the data of Forrestal and his colleagues (see Piekutowski et al. (1999) for example). We can see there post-mortem pictures of ogive-nosed steel rods impacting 6061-T651 aluminum targets, at velocities up to about 1.8 km/s, without any apparent deformation. In order to ensure convergence of the computations we have 11 cells on the projectile radius and a similar cell size (0.3 mm) along the target around its symmetry axis, up to a distance of about three projectile radii from the axis. The size of the cells at larger distances, towards the lateral surface of the target, is increasing geometrically as is customarily done in order to reduce computing times. We should note here that the use of Lagrange processor for the projectiles and Euler processor for the targets prevents cell mixing during the whole process and ensures a clear border between projectile and target. Moreover, the cells in the target do not deform because of the Eulerian meshing and those in the projectiles do not deform because of the high strength which we assign to them. Thus, the many difficulties which workers encounter with such simulations are avoided by this setup.

The constitutive relation which we use. for the target materials is the von-Mises yield criterion with no hardening or strain rate effects, in order to simplify the analysis. This criterion is adequate to describe the behavior of many steel and aluminum alloys whose stress–strain curves are very nearly elasto-pefectly-plastic, with a well defined flow stress. Moreover, these alloys are usually not very sensitive to strain rates, which mean that a dynamic test with a compression Kolsky bar is adequate to characterize their behavior, under most conditions encountered in terminal ballistics. An excellent example for these materials is the 6061T651 aluminum alloy which has been used by many workers (see Forrestal et al. (1991); Piekutowski et al. (1999) for example). As shown in (Forrestal et al., 1991) the static stress–strain curve for this material has a yield point at 0.276 GPa followed by a relatively short hardening behavior which reaches a roughly constant flow stress of 0.35 GPa. Dynamic stress–strain curves, using a Kolsky bar, result in a somewhat higher flow stress of about 0.4 GPa for this material. Thus, whenever we simulate this aluminum alloy we use a simple von Mises yield criterion with $Y = 0.4$ GPa for its strength. The dynamic compression tests, in a Kolsky bar system, are characterized by strain rates of (10^3–10^4 S^{-1}, which are the typical strain rates in a penetration process. Thus, one should use results from compression Kolsky bar tests as the input to the constitutive equations in the code, in order to match the strain rates and even the temperature increase, which the material experiences during a dynamic loading processes. The strain rates and the temperatures, as well as the strains which are achieved in these tests are very close to what the relevant target material, in the vicinity of the projectile, experiences. We do not specify any failure criteria for our targets because we focus on the penetration and perforation of ductile targets by sharp nosed projectiles through the ductile hole growth mechanism. The penetration in these cases is achieved by the projectile pushing the target material to the side and there is no need to introduce any fracture or failure process here. This is certainly not the case when blunt projectiles perforate very strong materials, like high strength steels, which can exhibit adiabatic shear or back surface spall failures. Thus, all the failure modes which may take place by fracture, shear-banding or other processes, are sidestepped here by considering only the ductile hole enlargement in our simulations. This, of course, limits the applicability of our results to cases where conical or ogive nosed projectiles perforate ductile metallic plates. We used the shock equation of state data in the AUTODN library, with a linear relation between the shock and particle velocities, for the materials involved in our simulations: aluminum, steel and tungsten with densities of 2.78, 7.9 and 18.5 g/cc, respectively. The sound velocities (C_0) and the slopes (S) of these linear shock relations are: $C_0 = 5.33, 4.57$ and 4.03 km/s and $S = 1.34$, 1.49 and 1.23 for Al, Fe and W, respectively. There are other options to use different equation of state, like the Gruneisen or the linear pressure-volume equations, but the shock equation seems to cover a larger pressure range in a more accurate way, so we always use it in our simulations.

3. The deep penetration of rigid short projectiles

As stated above, our first goal was to characterize the resisting stresses which a semi-infinite target exerts on a short rigid projectile. The best way to achieve this is to follow the time variation of the average deceleration, which the projectile experiences during deep penetration. We focus our attention on the ogive and spherical nosed projectiles, which represent the sharp and the blunt nosed projectiles, respectively.

3.1. Ogive-nosed projectiles

These short ($L/D = 3$) steel projectiles, with an ogive-nose (of 3CRH), can be considered as representing a typical AP projectile, which has L/D values of 3–5. We chose a low L/D value in order to enhance the effect of the entrance phase on these projectiles as we shall see below. Their diameter (6 mm) and their weight of 3.21 g result in an effective length of $L_{\text{eff}} = 14.4$ mm. The first set of simulations was performed with impact velocities of 0.5, 1.0 and 1.5 km/s at an aluminum target with strength of 0.4 GPa. From the results of (Rosenberg and Dekel, 2009) we know that these impact velocities are well below the critical velocity ($V_c = 2.1$ km/s) for this combination of target and projectile's nose shape. Thus, we expect these projectiles to be decelerated by a constant stress, $R_t = 1.87$ GPa (see (Rosenberg and Dekel, 2009)), when they penetrate deep enough, beyond the influence of the entrance phase. With the relation we derived in (Rosenberg and Dekel, 2009):

$$R_t = \rho_p \cdot L_{\text{eff}} \cdot a \tag{1}$$

we obtain a value of about $a = 1.65 \times 10^{-2})$ mm/$(\mu s)^2$ for the expected deceleration of these short steel projectiles, at deep penetration.

Fig. 1 shows the penetration and deceleration histories in these simulations from which several points are worth noting. First, it is clearly seen that at the low impact velocity (0.5 km/s) the projectile is stopped well before reaching a steady deceleration. This is a reasonable result considering the fact that it penetrates only 17 mm, which is much less than the value of 4–6D (24–36 mm), during which the effect of the entrance phases is expected to be dominant. The fact that the two penetration curves for the lower impact velocities show a decreasing trend after a certain time is due to the fact that we actually draw here the position of the projectile's nose. Since the target has a "spring-back effect" on the projectile we actually find it, in the simulations, in a somewhat backward position. However, the penetration depth is taken at the maxima in these curves. The penetration depths for the 1.5 km/s impact is high enough (78.5 mm), and Fig. 1b shows that the corresponding deceleration reaches the expected value derived above from Eq. (1). Moreover, the deceleration of this short projectile, beyond the entrance phase, is independent on its velocity. This is the same behavior we found in Rosenberg and Dekel (2009) for rigid long rods impacting semi-infinite targets at velocities below V_c.

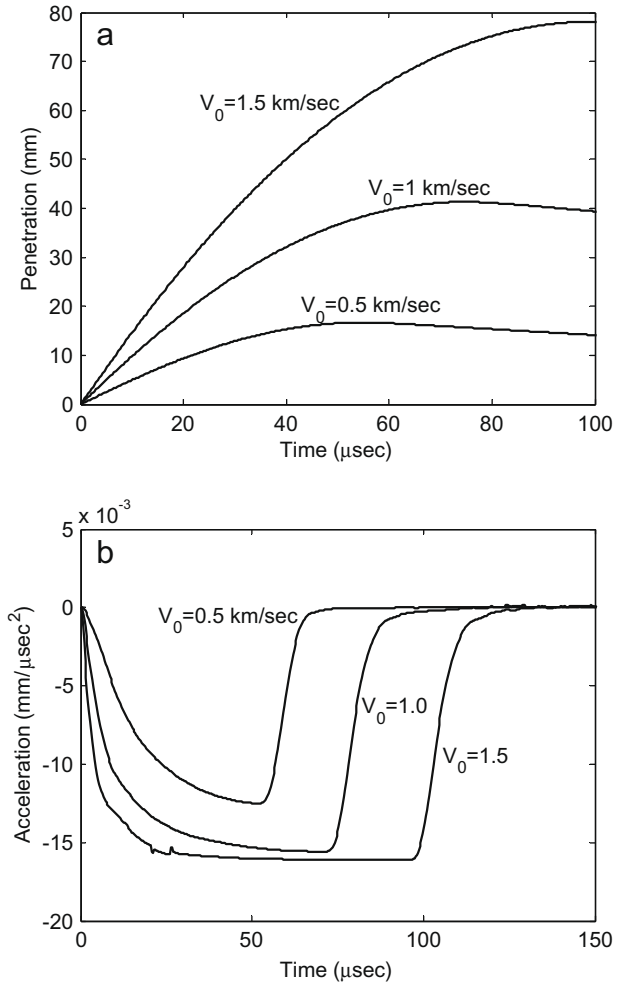

Fig. 1. (a) Penetration-time history and (b) deceleration time history for ogive nosed projectiles impacting the 0.4 GPa aluminum target at different velocities.

Examining the deceleration of the 1.5 km/s simulation, we see that the constant value is reached at about 25 μs after impact. From the penetration-time history, this time corresponds to a penetration depth of about 36 mm, exactly the 6D value. Moreover, one can observe a very fast increase of the deceleration, for the first 5 μs, followed by a more gradual increase for the next 20 μs. The short early part is due to the immersion process of the ogive nose in the target. The resisting force on the rod increases appreciably until its nose is fully embedded. The much longer, and more gradual increase in the deceleration, can be attributed to the diminishing effect of the impact face on the projectile, as it penetrates deeper into the target. This complexity of these deceleration histories means that any attempt to account for the resisting stresses on the projectiles, by using simplified analytical models, should be examined very carefully.

On the other hand, one can define an average (effective) stress, which the target exerts on the projectile, through an effective constant deceleration which it experiences during penetration. This effective deceleration (a_{eff}) of the projectile is obtained by the simple relation between its impact velocity (V_0) and penetration depth (P), for a motion at constant deceleration:

$$a_{\text{eff}} = V_0^2/2P \tag{2}$$

Using Eq. (2) with the values for the penetration depths, in the three simulations described above, we get the following effective decelerations: $a_{\text{eff}} = 0.714$, 1.2 and 1.43×10^{-2} mm/(μs)^2, for the impact velocities of: $V_0 = 0.5, 1.0$ and 1.5 km/s, respectively. These values are lower than the asymptotic value we predicted from Eq. (1) for the deceleration at deep penetration, $a = 1.65 \times 10^{-2}$ mm/(μs)^2, but they are approaching it with increasing impact velocity. One can insert these effective decelerations (a_{eff}) in Eq. (1) to obtain the corresponding effective (average) stresses which the target exerts on the projectile at these velocities: σ_r=0.81, 1.36 and 1.63 GPa, for the impact velocities of 0.5, 1.0 and 1.5 km/s, respectively. These values increase asymptotically towards the expected value of R_t (1.87 GPa) for an ogive nosed projectile at deep penetration in this aluminum target. It is important to note that this increase in the effective resisting stress, with impact velocity is due to the effect of the free impact face, which exerts a low resisting force on the projectile. This increase is not the result of any velocity dependent term in the resisting stress, as we demonstrated in (Rosenberg and Dekel, 2009). It would be very difficult to find a quadratic relation between these effective stresses and the projectile velocity (V), of the form:

$$\sigma_r = R_t + BV^2 \tag{3}$$

which is the basic equation in all the analytical models relying on the dynamic cavity expansion analysis since Goodier's work (Goodier, 1965).

At this point we bring an example from the experimental results of Dikshit and Sundararajan (1992), for short (L/D = 2.5) ogive nosed steel projectiles, impacting 80 mm thick steel plates at velocities of up to 800 m/s. The yield strength of their steel targets was about 0.8 GPa. As the maximum penetration depth in this series of shots, was less than half the target thickness, one can treat these plates as semi-infinite. The measured depths of penetration were: 12.7, 21 and 29 mm, for impact velocities of 300, 500 and 700 m/s, respectively. Using Eq. (2) for the effective decelerations in these shots we obtain: $a_{\text{eff}} = 3.54$, 5.95 and 8.45×10^{-3} mm/(μs)^2. These values are related to the corresponding impact velocities by an almost linear manner, which means that they are still far from their asymptotic value. From our results in Rosenberg and Dekel (2009), for such ogive nosed projectiles penetrating 0.8 GPa steel targets, we get a value of $a = 12 \times 10^{-3}$ mm/(μs)^2 for the asymptotic deceleration, which these projectiles should experience at deep penetration. This value is higher by more than 40% than the maximum effective deceleration we calculated above (at impact velocity of 700 m/s). Thus, it is clear that the entrance phase dominates all the results in Dikshit and Sundararajan (1992).

In order to further highlight the role of the entrance phase we performed another set of simulations, in which we introduced a cylindrical hole from the impact face to a depth of 50 mm in the target. The diameter of this cavity was 6.1 mm, slightly larger than that of the projectile, so that the projectiles in these simulations do not "see" the free face of the target. The idea here is that the impact, at a depth of 50 mm, prevents the target surfaces from moving, because of the presence of the projectile inside the hole. Thus, we expect the penetration depths to be smaller than the corresponding depths with the flat faced targets. We also expect their deceleration histories to be much less influenced by the entrance phase, reaching their asymptotic values, at much earlier times. We obtained penetration depths of 14, 37.8 and 74.6 mm for the 0.5, 1.0 and 1.5 km/s impacts, respectively which are smaller by about 23%, 10% and 5% than the corresponding penetrations into flat faced targets. Fig. 2 shows the deceleration time histories in these simulations, together with those for the flat faced targets. It is quite clear that with higher impact velocities the differences between the deceleration histories diminish. The large difference for the 0.5 km/s impact, in both the shape and the amplitude of these deceleration histories, means that the entrance phase is dominant here, as discussed above.

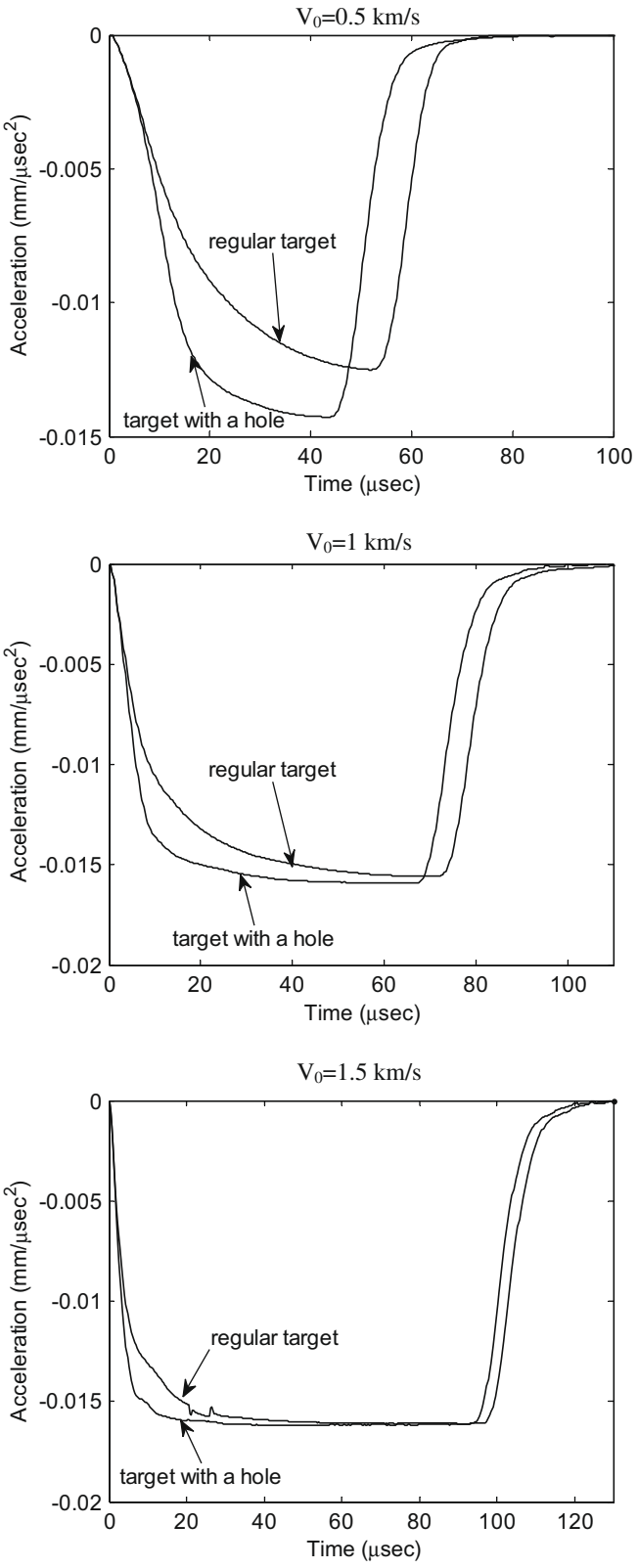

Fig. 2. Deceleration-time histories for the ogive nosed projectiles impacting flat faced targets and targets with a hole at different velocities.

3.2. Spherical-nosed projectiles

A similar series of simulations was performed with spherical nosed $L/D = 3$ steel rods, impacting 0.4 GPa aluminum targets, both flat-faced and with the 50 mm deep hole, at velocities of 0.5, 1.0 and 1.5 km/s. The effective length of this projectile is $L_{\text{eff}} = 17$ mm. Using the value we found in (Rosenberg and Dekel, 2009) of $R_t = 2.244$ GPa, for spherical-nosed rods impacting the 0.4 GPa aluminum target, we get from Eq.(1) a value of $a = 0.0167\ \text{mm}/(\mu\text{s})^2$ for the asymptotic deceleration of these

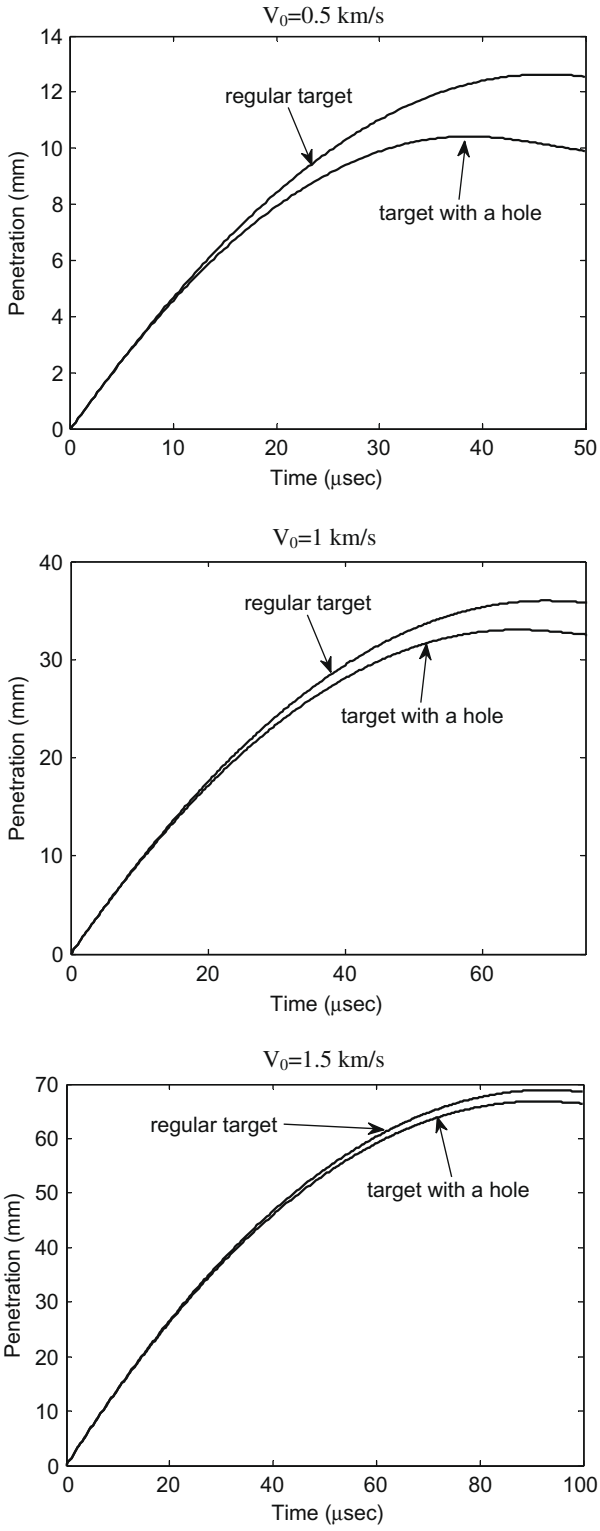

Fig. 3. Penetration-time histories for spherical nosed projectile impacting the flat target and the target with the hole at different velocities.

short projectiles at deep penetration. Fig. 3 shows simulation results for the penetration depth histories in the two targets. Penetration depths in the target with the hole are smaller, as expected, and the differences between the two sets also diminish with impact velocities. These differences are somewhat smaller than those for the ogive projectile: 21%, 8.4% and 3.3% for impact velocities of 0.5, 1.0 and 1.5 km/s, respectively. This may be due to the fact that the spherical nose is shorter than the ogive nose and it is fully immersed in the target at shorter times. Still, most of the difference between the penetration into a flat target and one with a hole is due to the effect of the entrance phase, after the nose is fully embedded in the target.

Fig. 4 shows the deceleration histories of these projectiles at the three impact velocities into the two targets. As expected, the projectile experiences a higher deceleration with the hole in the target and the difference in decelerations is diminishing with increasing impact velocities. The simulation for the 0.5 km/s impact shows that the deceleration does not reach a constant value during the short penetration time, as in the case of the ogive nosed projectile. With the 1.0 km/s impact the entrance phase lasts for more than 20 μs, which is a third of the total penetration phase. Thus, as for the ogive nose, the forces on these short projectiles are varying considerably during the entrance phase, which is most significant for impact velocities in the 0–1.0 km/s range. A close examination of the early parts in the deceleration histories shows that the steep initial part lasts for a few microseconds which correspond to the embedment of the spherical nose in the target. The following, more gradual change in deceleration, lasts until the projectile has penetrated about six rod diameters, as in the case of ogive nosed projectiles.

3.3. A few words about the constant deceleration of rigid projectiles

The previous simulations showed that at deep penetrations a short projectile experiences a constant resisting stress, in agreement with our previous findings in (Rosenberg and Dekel, 2009) for rigid long rods. This conclusion contradicts the common assumption that rigid projectiles are decelerated by forces which depend on both target strength and inertia, as given by Eq. (3). The addition of target inertia to the resisting force, through the dynamic cavity expansion analysis, was first suggested by Goodier (1965) who analyzed penetration data for various spheres into semi-infinite targets made of steel, aluminum etc. Analytical models, for the penetration process of rigid long rods, follow the same lines by assuming that the resisting force on these rods are dependent on both target strength and inertia (see Forrestal et al. (1991); Piekutowski et al. (1999), for example). In this section we wish to highlight some facts in order to understand the source of the discrepancy between our approach, with the constant deceleration, and the approach which is based on the dynamic cavity expansion and includes target inertia..

A close examination of the data which Goodier (1965) used for his model (see the survey in (Hermann and Jones, 1961)), shows that it includes spheres made of copper, aluminum, steel and lead at impact velocities of up to 1.5 km/s. These spheres penetrated much less than Goodier predicted by a constant resisting stress, which depends on target strength only. Thus, he added the inertia term to the target resistance, in order to account for these low penetration depths, treating the spheres as rigid in his model. Clearly, the spheres used in (Hermann and Jones, 1961) did not stay rigid during these experiments, and their low penetration depths were due to their strong deformation rather than the inertia of the target. Thus, the main reason for the addition of target inertia to the resisting force on these projectiles is based on a flawed assumption on Goodier's part, namely, that the spheres in these experiments were rigid. The data of Weimann (from EMI laboratories), as it appears in (Dehn, 1986), clearly shows the difference between soft and hardened steel spheres impacting aluminum targets. The hard steel spheres penetrate much more than the soft ones, as expected. Thus, we may conclude that the addition of a velocity dependent term (inertia), to the resisting force on rigid projectiles, cannot be justified by the experimental results of Hermann and Jones (1961).

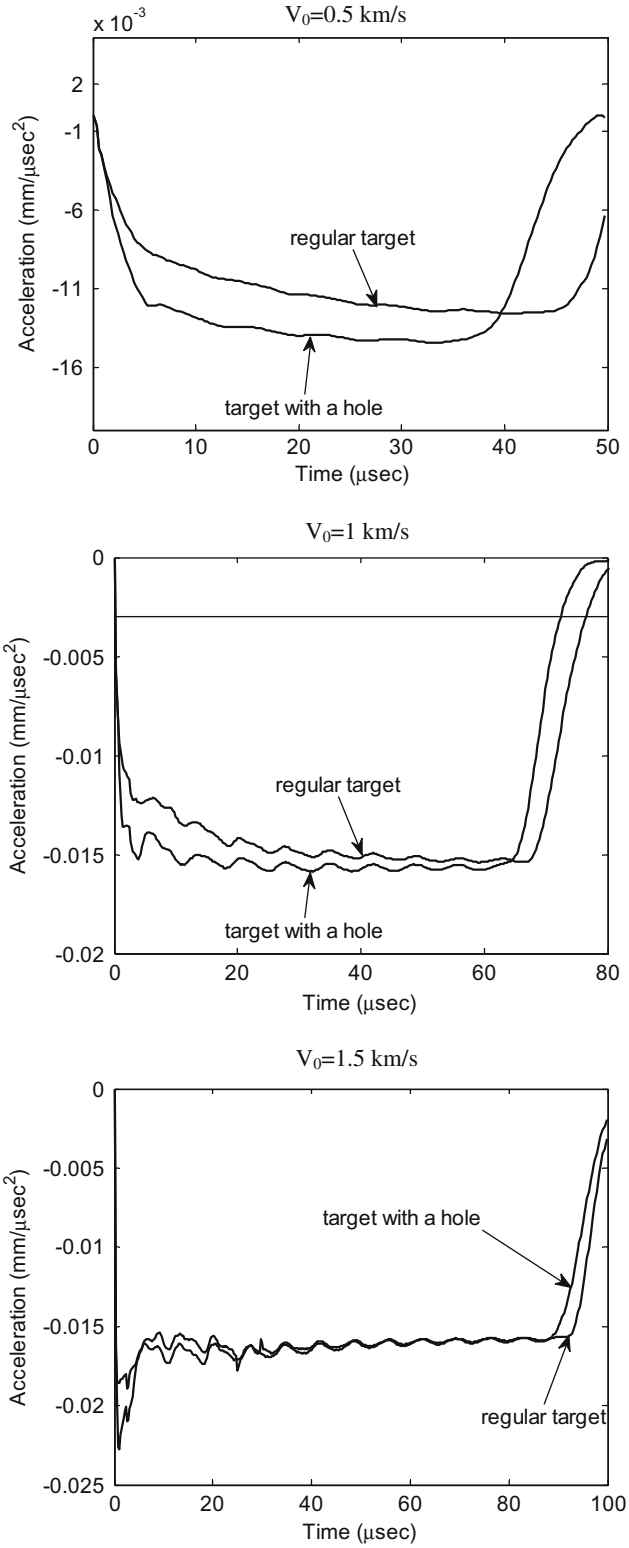

Fig. 4. Deceleration-time histories for the spherical nosed projectiles in both targets.

The direct experimental determination of a projectile's deceleration is very complex and there were very few attempts to achieve such measurements in the past. One of them is the study by Forrestal et al. (2003) where the deceleration of rigid rods, as they penetrate concrete targets, was measured with special gauges embedded in the rods. There are several measurements of these decelerations in (Forrestal et al., 2003), for two types of concrete, but none of them really matches their model predictions, as far as the shape of the signals is concerned. The authors of Forrestal et al. (2003) claim that they do not see evidence for target inertia playing any role in these measurements. They state that "the inertial term will, however, become much more important for larger striking velocities" as for the data in (Piekutowski et al., 1999). However, a close examination of the data in (Piekutowski et al., 1999), for ogive nosed steel rods impacting 6061-T651 targets, reveals a different picture. Using Eq. (2) for the effective deceleration for each test in (Piekutowski et al., 1999) we find that, except for the very lowest impact velocities, these decelerations are practically constant with values of: $a_{\text{eff}} = (3.58 \pm 0.38) \times 10^{-3}$ mm/(μs)^2. The corresponding impact velocities, between 679 and 1786 m/s, span a large range but we do not see any evidence for a velocity dependent deceleration in these results. In fact, even for the lowest impact velocity (570 m/s) the effective deceleration is only slightly less – 2.95×10^{-3} mm/(μs)^2, due to the enhanced influence of the entrance phase in this shot. Thus, the data of Piekutowski et al. (1999) does not justify the addition of the inertial term to the target's resistance to penetration. In fact, we showed in (Rosenberg and Dekel, 2009) that a similar conclusion can be reached by analyzing the data for concrete targets penetrated by rigid rods.

4. Plate perforation and residual velocities

A vast amount of empirical data has been gathered over the past 50 years on the perforation of finite thickness plates by various projectiles and long rods. Different projectile nose shapes, as well as target properties and thicknesses, result in different perforation mechanisms which include: ductile hole enlargement, perforation by shearing and plugging, back surface spall, petalling etc. Depending on whether thin or thick plates are used, their properties (ductile or brittle) and projectile nose shape (blunt or sharp), one can get a different mechanism at work, as discussed by Recht and Ipson (1963). In this study we focus our attention on rigid, sharp nosed projectiles (ogive and conical), which perforate ductile targets by the process of ductile hole enlargement.

Two recent papers, by Chen et al. (2008) and by Forrestal and Warren (2009), present analytical models to account for a large number of experimental results for the perforation of metallic targets by rigid projectiles and rods. The analysis in both works is based on the dynamic cavity expansion, according to which the resisting stresses on these projectiles are velocity dependent. The expressions and values of these stresses are taken from the earlier works of Forrestal and his colleagues on the deep penetration of rigid long rods into semi-infinite targets. In the previous sections we discussed the significant effect which the entrance phase has on the penetration process of short projectiles. For thin plate perforation we expect the back surface of the target to play an additional role, by further reducing the resisting stresses on the projectile. Thus, a simple picture, where a constant resisting stress is acting on the projectile as it perforates a finite thickness target, must be very naive. In order to highlight this issue we performed several simulations of the perforation experiments which have been discussed in (Chen et al., 2008; Forrestal and Warren, 2009). The results from these simulations will be described in view of the simple model suggested by Recht and Ipson (1963).

4.1. Perforation by conical-nosed projectiles-simulation results

We start this section by presenting our simulation results for conical-nosed tungsten projectiles, with $D = 8.3$ mm and $L_{\text{eff}} = 25.6$ mm, impacting aluminum plates. The thicknesses of the plates, $H = 12.7$, 50.8 and 76.2 mm, as well as the shape of the conical projectile and its density (18.5 g/cc), are the same as those in the experiments of Forrestal et al. (1990). The yield strength of their aluminum 5083-H131 targets was 0.276 GPa and the flow stress about 0.4 GPa, as shown in (Forrestal et al., 1990). Thus, as we explained above, we chose the value of 0.4 GPa for the strength of the targets in our simulations, using a von-Mises yield criterion. Moreover, the compressive stress–strain curve for this alloy extends to a strain of about 1.0, with no sign for material failure (see Forrestal et al. (1990)). We performed several simulations with a failure strain of 1.0 and compared them to the simulations with no failure strain. The difference between the residual velocities of the two sets was only about 2–3%. Thus, we performed our study without specifying a failure strain to the targets. As the projectiles in (Forrestal et al., 1990) did not deform in all the experiments, we assigned them a high strength (50 GPa), in order to ensure their rigidity.

The first set of simulations was performed for an impact velocity of 800 m/s, and the resulting residual velocities were: $V_r = 769, 603,$ and 422 m/s for the 12.7, 50.8, and 76.2 mm plates, respectively. These values are very close to the experimental results in (Forrestal et al., 1990): $V_r = 761, 591$ and 421 m/s, for these plates. This agreement means that the value we chose for the target strength in our simulations (0.4 GPa) is close to the flow stress of the aluminum plates used in (Forrestal et al., 1990). Fig. 5 shows the resulting decelerations which the projectile experiences during its penetration through these targets. The effect of the target's free faces is very clear, as expected. We can even identify the time when the conical-nose is embedded in the target, as shown in the figure by the arrow. The most important conclusion which we draw from these results, is that the decelerations and the resisting stresses, which these targets exert on the projectile, are very different from each other, both in their shape and magnitude. This means that a simple analytical model, which is based on these stresses, must be very difficult to construct.

The next set of simulations was performed with other impact velocities on the same targets, adding two more plates ($H = 8.3$ mm and 100 mm), in order to cover a larger range of target thicknesses. Table 1 summarizes the results of these simulations in

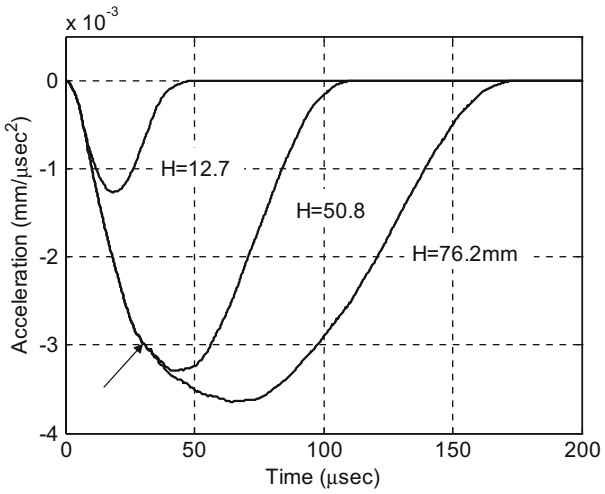

Fig. 5. Deceleration-time histories for the conical-nosed tungsten projectiles impacting the three aluminum plates at 800 m/s.

Table 1
Simulation results for V_r of the conical-nosed tungsten projectiles perforating aluminum plates of different thicknesses.

H (mm)	V_0 (m/s)	V_r (m/s)
8.3	200	106.1
	300	249
12.7	300	207
	500	449
	800	769
50.8	600	284.4
	800	602.6
	1000	842
76.2	800	422
	1000	723.6
	1200	975
100	800	116.6
	1200	874.6

terms of the residual velocity (V_r) as function of impact velocity (V_0) and plate thickness (H):

Our next step is to use the values in Table 1 as a validation means for the simple analytical model of Recht and Ipson (1963). Their analysis of the perforation process by sharp nosed projectiles is based on energy conservation, resulting in the following relation betweenV_0, V_r and the ballistic limit velocity (V_{bl}):

$$V_r^2 = V_0^2 - V_{bl}^2 \tag{4}$$

The basic assumption of Recht and Ipson (1963) is that the work needed to perforate a given ductile plate, by a sharp projectile, is constant. They write that "while the assumption of constant perforation work is not justified, this equation (Eq. (4)) seems to represent the data to velocities exceeding V_{bl} by at least 50%". Our simulations can be used as a verification test for this assumption for a larger range of impact velocities. We start this validity check through the values we infer for V_{bl} at different impact velocities. Using the tabulated values of V_0 and V_r for the five plates in Table 1, we get from Eq. (4) the inferred V_{bl} values which are given in Table 2 below.

One can clearly see that, for each plate thickness, the different impact velocities resulted in practically the same values for V_{bl}. The small differences within each set (less than 2%) are probably due to the different kinetic energies which the projectiles impart to the targets. In fact, the code also lists the energy invested in the target (the plastic work) after the perforation process. It turns out that these energies are practically velocity independent and they only depend on the thickness of the plate in these simulations. This means that the simple analysis of (Recht and Ipson, 1963) is good enough for a large range of velocities and the only important quantity is the plastic work which is needed to perforate a given target. This work is a function of target strength and thickness but it does not depend on impact velocity.

At this stage we introduce a new concept which, as will be shown here, is very useful for the analysis of perforation experiments. This is the effective resisting stresses, which is exerted on the projectile during perforation. Our basic assumption is that there is no need to follow the complex temporal changes of the stresses on the projectile. Instead, one can assign an effective stress (σ_r), for each plate thickness, which results in the same change in projectile velocity. This means that the equation of motion (Newton) of the projectile is:

$$\rho_p \cdot L_{eff} \cdot dV/dt = -\sigma_r = \text{const.} \tag{5}$$

Using the well known relation: $dV/dt = VdV/dx$, together with the boundary conditions: $V_0 = V_{bl}$ at $x = 0$ and $V = 0$ at $x = H$, we get after the integration:

$$\rho_p \cdot L_{eff} \cdot V_{bl}^2 = 2H\sigma_r \tag{6}$$

Thus, given a value for V_{bl} we can calculate the effective resisting stress (σ_r), which a target of thickness H exerts on the projectile during perforation, at any impact velocity. While σ_r should be independent on impact velocity, because V_{bl} is independent on V_0, it should depend on target strength, and possibly on its thickness. Moreover, we assume that the important parameter here is the ratio – H/D – of plate thickness to projectile diameter. Our simulations results, to be presented here, will test this assumption. Using the values for the inferred V_{bl} (Table 2), together ρ_p (18.5 g/cc) and L_{eff} (25.6 mm), we get the following effective stresses, as a function of plate thickness, from Eq. (7): which is a different way to write Eq. (6):

$$\sigma_r = \rho_p \cdot L_{eff} \cdot V_{bl}^2/2H \tag{7}$$

It is clearly seen that the effective stresses increase in an asymptotic manner as the ratio H/D increases. We can assume that for very high H/D values σ_r reach the corresponding value of R_t, the resistance to penetration in a semi-infinite target. In order to find the value of R_t for these conical-nosed tungsten projectiles we performed another simulation of an impact at 800 m/s, on a very thick aluminum target with a strength of 0.4 GPa. Fig. 6 shows the resulting deceleration-time history of the projectile in this simulation, together with that for the 100 mm target. Clearly, even this relatively large thickness (with $H/D = 12$) is not large enough to reach a constant deceleration for the projectile. We see that the first part of the penetration is affected by the front surface and the second half by the back face of the target. In contrast, for the semi-infinite target the deceleration reaches a constant value, of $a = 4.0 \times 10^{-3}$ mm/(μs)^2, after the entrance phase is over. The fact that this tungsten projectile reached

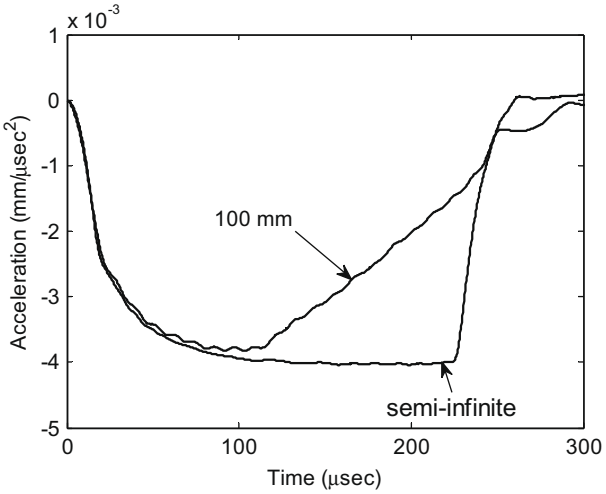

Fig. 6. The deceleration-time histories for the conical-nosed tungsten projectile impacting a semi-infinite and a 100 mm thick aluminum targets (with strength of 0.4 GPa), at 800 m/s.

Table 2
Inferred V_{bl} values for the five plate thicknesses.

H (mm)	8.3	12.7	50.8	76.2	100
V_{bl}(m/s)	168±1.5	219±2	533±6	690±10	807±15

Table 3
The effective resisting stresses as derived from Eq. (7) and Table 2.

H (mm)	8.3	12.7	50.8	76.2	100
H/D	1	1.53	6.12	9.18	12
σ_r (GPa)	0.805	0.894	1.32	1.48	1.54

Table 4
Experimental results for the 12.7 mm plates and the inferred V_{bl} values.

V_0 (m/s)	221	278	290	479	532	726	892	1023	1195
V_r (m/s)	0	142	177	412	464	684	895	989	1156
V_{bl} (m/s)	–	239	229.7	244	260	243	240	261	302.8

Table 5
Experimental results for the 50.8 mm plates and the inferred V_{bl} values.

V_0 (m/s)	513	573	578	590	655	810	1037	1176
V_r (m/s)	0	242	250	255	378	595	863	1022
V_{bl} (m/s)	–	519	521	547.7	540	550	575	582

Table 6
Experimental results for the 76.2 mm plates and the inferred V_{bl} values.

V_0 (m/s)	635	690	709	792	959	1021	1168
V_r (m/s)	0	169	248	420	667	767	889
V_{bl} (m/s)	–	669	664	671.5	689	674	757

a constant deceleration is due to its high density which resulted in a considerably higher penetration as compared with the steel projectiles we discussed earlier. Thus, the deep penetration of short projectiles is also characterized by a constant deceleration, without target inertia effects, as we found for long rods. Using Eq. (1), and this value of deceleration, together with ρ_p=18.5 g/cc and $L_{eff} = 25.6$ mm, we get: $R_t = 1.894$ GPa for this conical-nosed projectile penetrating the 0.4 GPa aluminum target. This value is very close to the value of $R_t = 1.944$ GPa which we obtained in (Rosenberg and Dekel, 2009) for a conical-nosed long rod, with a somewhat larger cone angle, penetrating the same target. The effective stresses (σ_r), for all the plates in our simulations (see Table 3), are much lower than this value of R_t, due to the strong effects of the target's free faces.

4.2. Analysis of experimental data

The next step is to analyze the experimental results of Forrestal et al. (1990), for the same conical-nosed tungsten projectiles perforating the 12.7, 50.8 and 76.2 mm thick aluminum 5083-H131 plates. The following tables (4, 5 and 6) include the impact velocity (V_0) and the residual velocity (V_r), for all the experiments in (Forrestal et al., 1990), together with the inferred ballistic limit velocity (V_{bl}), from Eq. (4), for each plate thickness.

Several important points emerge by examining the inferred V_{bl} values in these tables. First, it is clear that some experiments result in "strange" values for the inferred V_{bl}, which are outside the experimental range for V_{bl}. For example, the values for V_{bl} in the last shots for the 12.7 mm plate (302.8 m/s) and the 76.2 mm plate (757 m/s), are clearly too high. The same is true for the two experiments with the highest impact velocity for the 50.8 mm plate. Clearly, the inferred values for V_{bl} should not be higher than the minimal velocities for which these plates have been penetrated. A possible explanation for this discrepancy is that the way we infer the values for V_{bl} from the data, is very sensitive to experimental errors at high velocities. A reasonable estimate of this error is about 2% for the residual velocity and about 1% for the impact velocity. Thus, an increase by 2% in V_r, in the last shot for the 50.8 mm plate, results in a new inferred value of $V_{bl} = 545$ m/s, which is well within the permitted range for V_{bl} from the data. In order to avoid such corrections we decided to ignore these few "strange" data points, for the moment, and obtained the following average values of V_{bl} for the three sets. We also included the range of impact velocities where these V_{bl} should be located, according to the data in each set:

$$V_{bl} = 245 \pm 15 \text{ m/s} \quad \text{for the 12.7 mm plate } (221 < V_{bl} < 278)$$
$$V_{bl} = 535.5 \pm 15 \text{ m/s} \quad \text{for the 50.8 mm plate } (513 < V_{bl} < 573)$$
$$V_{bl} = 664.5 \pm 12 \text{ m/s} \quad \text{for the 76.2 mm plate } (635 < V_{bl} < 690)$$

We should note that the relative scatter in these three cases is small enough and that it is decreasing with plate thickness. However, the most important observation is that the inferred values for V_{bl} do not depend on impact velocity within each group. As discussed above this is a clear indication that the simple model of (Recht and Ipson, 1963), is valid for these cases. Next we calculate the effective resisting stresses which these plates exert on the conical projectiles through Eq. (7), using the inferred V_{bl} values listed above. The values we get are: σ_r=1.12, 1.33 and 1.37 GPa for the 12.7, 50.8 and 76.2 mm plates, respectively. These values are quite close to those which we derived for σ_r from the simulations above (see Table 3). As with the simulation results, these effective stresses (σ_r) are also increasing with plate thickness and their values seem to approach an asymptotic value(R_t) for deep penetration.

Another set of experiments with conical-nosed steel projectiles, 20 mm in diameter, perforating aluminum plates, was given in Borvik et al. (2004). The aluminum alloy was AA5083-H116 and plate thicknesses were 15, 20, 25 and 30 mm. There was a measurable difference between the stress–strain curves for samples taken from these plates. The 20 and 30 mm plates had the same flow stresses, while the 25 mm plate was weaker by about 10% and the 15 mm plate was stronger by the same amount. Using Eq. (4) and the tabulated values for the impact and residual velocities in (Borvik et al., 2004), one obtains: $V_{bl} = 215$, 246, 257 and 310 m/s, for the 15, 20, 25 and 30 mm plates, respectively. With the projectile's effective length of $L_{eff} = 78$ mm, we get from Eq. (7): σ_r=0.94, 0.93, 0.81 and 0.98 GPa, for the 15, 20, 25 and 30 mm plates, respectively. One can clearly see the lower σ_r for the 25 mm plate, as expected. We shall come back to this set of experiments later on (in Section 5.5).

4.3. Perforation by rigid rods

The data analyzed in (Chen et al., 2008; Forrestal and Warren, 2009) include several sets of perforation studies with ogive and conical-nosed steel rods impacting thin aluminum plates. We wish to check the applicability of our analysis for these cases and to highlight the different qualities of these experimental results. The three sets of data which we compare were reported by Piekutowski et al. (1996), Forrestal et al. (1987), Rosenberg and Forrestal (1988). These works used aluminum 6061-T651 plates, 26.3 mm thick in (Piekutowski et al., 1996) and 25.4 mm in (Forrestal et al., 1987; Rosenberg and Forrestal, 1988). The rods were ogive-nosed in (Piekutowski et al., 1996) (D=12.9 mm, $L_{eff} = 79.2$ mm), and conical-nosed in (Forrestal et al., 1987) (D=9.53 mm, $L_{eff} = 136.5$ mm) and in (Rosenberg and Forrestal,

Table 7
The experimental results from (Piekutowski et al., 1996) and the inferred $\mathbf{V_{bl}}$ **values**.

V_0 (m/s)	282	308	341	396	454	508	565	630	633	730	863
V_r (m/s)	0	57	164	266	347	415	482	555	561	665	802
V_{bl} (m/s)	–	302.7	299	293.3	292.7	293	294.8	298	293.2	301	318.7

1988) (D=7.1 mm, $L_{eff} = 74.6$ mm). Thus, the corresponding H/D values for the three sets of experiments are: $H/D = 2.04$ in (Piekutowski et al., 1996), 2.66 in (Forrestal et al., 1987), and 3.58 in (Rosenberg and Forrestal, 1988). The following tables list the relevant data from these works, as far as V_0 and V_r are concerned together with the values inferred for V_{bl} from each shot (by Eq. (4)):

Comparing the inferred V_{bl} values in these tables one can see the differences in the quality of the data. All the values for V_{bl} from (Piekutowski et al., 1996) (Table 7), except for the last shot, fall within the range $V_{bl} = 297.5 \pm 5$ m/s. The last shot is also a "strange" one, as defined above, and we do not include it in the averaging process. This set of data is certainly of excellent quality, with a very small variation of the inferred V_{bl} values, enhancing our claim that the simple model of Recht and Ipson (1963) is accurate enough. The same conclusion holds for the results of Forrestal et al. (1987) (Table 8) where, except for the highest impact velocity, all the inferred ballistic limit velocities fall in the range of $V_{bl} = 235 \pm 7.5$ m/s. In contrast, the third set of experiments (Table 9), from Ref (Rosenberg and Forrestal, 1988), is very problematic, to say the least. Out of the eight shots above the ballistic limit, only the first four result in V_{bl} values which are within the permitted range of 327–383 m/s. Moreover, V_{bl} from these four shots span a very large range between 318 and 341 m/s. To our best understanding this is the result of large error bars on both V_0 and V_r in these shots, which were actually performed by one of us (Z.R.), so he has no one else to blame. It is important to compare these sets of experiments in order to demonstrate the variability in the quality of published data. One can also calculate the effective resisting stresses for the experiments in (Piekutowski et al., 1996; Forrestal et al., 1987) by using the average values for V_{bl}, as given above. Using Eq. (7) with the corresponding values for L_{eff}, H and V_{bl}, we get σ_r=1.046 GPa for the plates in (Piekutowski et al., 1996) with $H/D = 2.04$, and σ_r=1.19 GPa for plates in (Forrestal et al., 1987) with $H/D = 2.66$. These σ_r values agree with those we found in our simulations for the conical projectiles perforating 0.4 GPa aluminum plates (see Table 3) because the strength of the 6061-T651 alloy is very close to 0.4 GPa.

4.4. More observations regarding perforation experiments

The simple relation (Eq. (4)) between the three relevant velocities V_0, V_r and V_{bl} was justified by both our simulations, and the experimental data which we analyzed here. In the present section we wish to highlight some general observations, which may be useful for the cases we discussed here, namely, ductile targets perforated by sharp projectiles. The first thing is to realize that V_r is always smaller than V_0 and that it must approach this value asymptotically at high impact velocities. This may seem as a trivial statement but one should note that it is true only for targets which are penetrated by the ductile hole enlargement process. Other perforation mechanisms, such as plug formation, do not show this behavior since the kinetic energy of the plug has to be taken into account. Thus, we expect that the $V_r = V_r(V_0)$ curves for those cases should keep a certain distance from the line $V_r = V_0$, rather than to merge towards it. This difference between the two mechanisms can be clearly seen in the experimental results of Borvik et al. (2002) who measured the residual velocities of both blunt and conical-nosed rigid projectiles perforating the same steel targets.

Another point to note is that by differentiating equation (4) we get the slope of the V_r vs.V_0 curve as $dV_r/dV_0 = V_0/V_r$. Thus, as V_r approaches zero the slope is infinite and the curve is perpendicular to the V_0 axis at V_{bl}. This means that small changes in impact velocity, just above the ballistic limit, can result in large changes in the residual velocities. With increasing impact velocities the slope of the curve decreases, reaching a value of one in an asymptotic manner. As far as the sensitivity to experimental errors is concerned we have from Eq. (4)

$$\delta V_{bl} = (V_0/V_{bl})\delta V_0 + (V_r/V_{bl})\delta V_r \tag{8}$$

where the δ signs stand for the errors in the corresponding variables. This equation means that the higher the impact velocity (with correspondingly higher residual velocity) the larger is the error in V_{bl} from Eq. (4). This is probably the main reason for all those "strange" results at the highest impact velocities in the tables above. This increased sensitivity of V_{bl} to the errors in V_0 and V_r, at high impact velocities, is due to the factors V_0/V_{bl} and V_r/V_{bl} which multiply δV_0 and δV_r in Eq. (8). Thus, the importance of measurement accuracy is enhanced at the high velocity range. Another example for this issue is given in the data of Borvik et al. (2002) for conical-nosed steel projectiles, with a diameter of 20 mm, perforating 12 mm Weldox 460E steel plates. The two shots at $V_0 = 300.3$ m/s ($V_r = 110.3$ m/s) and $V_0 = 280.9$ m/s ($V_r = 0$) are used by the authors to determine the ballistic limit velocity at $V_{bl} = 290.6$ m/s. However, using Eq. (4) it turns out that, except for the highest impact velocity ($V_0 = 405.7$ m/s), the inferred V_{bl} is closer to 275 m/s. This value is very close to the highest impact velocity for which the projectile did not penetrate the target ($V_0 = 280.9$ m/s). The small difference between these two values is certainly within the error bars on these measurements, as we discussed above.

The most important issue here is that all the physics of the perforation process lies in the determination of V_{bl}. This is easily seen by rewriting Eq. (4) in its normalized form, as suggested in (Recht and Ipson, 1963):

$$V_r/V_{bl} = \left[(V_0/V_{bl})^2 - 1\right]^{0.5} \tag{9}$$

Thus, a single normalized curve should be adequate to represent all perforation experiments, with sharp nosed projectiles and ductile targets. The only difference between various sets of data is in the value of V_{bl} which is unique to each projectile/target pair. The obvious consequence of this result is that there is no need to perform a lot of perforation experiments in order to determine the $V_r = V_r(V_0)$ curve for a given target/projectile combination. Rather, the ballistic limit should be accurately determined and the rest of the curve, at high velocities, can be safely drawn through this normalized relation. For the determination of V_{bl}, it is enough, in principle, to perform a single experiment in which V_0 and V_r are accurately measured, and then use Eq. (4) to determine V_{bl}. We have seen that at impact velocities near V_{bl} we expect large changes in V_r, while at high impact velocities the errors in the measured V_0 and V_r, may result in large errors in the inferred V_{bl}. Thus, the best way to determine V_{bl}, from a single experiment, is to perform it with an impact velocity of (1.5–2) V_{bl}. In order to demonstrate the validity of this normalized scheme we show in Fig. 7 all the data from Forrestal et al. (1990), for the conical-nosed tungsten projectiles perforating

Table 8
The experimental results from Forrestal et al. (1987) and the inferred V_{bl}values.

V_0 (m/s)	213	254	272	315	344	537	691
V_r (m/s)	0	80	141	207	258	479	640
V_{bl} (m/s)	–	241	232.6	237.4	227.5	242.7	260.5

Table 9
The experimental results from Rosenberg and Forrestal (1988) and the inferred V_{bl} values.

V_0 (m/s)	327	383	419	515	886	1394	1442	1516	1575
V_r (m/s)	0	175	260	399	827	1334	1397	1445	1509
V_{bl} (m/s)	–	340.7	318.6	325.6	318	404	357.5	458	451

the three aluminum plates (5083-H131) with the different thicknesses. We also added the data from Piekutowski et al. (1996) and Forrestal et al. (1987) for the ogive and conical-nosed rods perforating the 6061 and T651 aluminum plates. The values for V_{bl} are those we inferred above, through the averaging process (disregarding the "strange" results). Still, even the experimental results from these "strange" shots are included in Fig. 7. It is quite clear from this figure that all the data, including the "strange" results, can indeed be represented by the universal curve, with its normalized velocities, through Eq. (9).

5. A short parametric study of the effective resisting stress (σ_r)

5.1. The need for numerical simulations

As stated above, the only challenging scientific issue, in the perforation process of ductile plates, is to account for the value of V_{bl} (or σ_r), for a given projectile/target pair, through an analytical model. A good way to avoid the complexity of analytical models, and still learn a lot about a given process, is to use numerical simulations where each parameter can be changed within a large range, while holding the other parameters constant. In this section we present such a numerical study which may help in building a physically based analytical model for σ_r. Before describing the results of these simulations, we should note that the previous simulations, as well as the experimental data, show that σ_r increases from a value of about 2Y, for plates with $H/D = 1$, to about 4Y at $H/D = 10$. This increase, as well as the asymptotic approach of σ_r to R_t, at large thicknesses, are the main challenge to the modeler. The result for the $H/D = 1$ plates is in excellent agreement with early works by Bethe (1941) (from the days of W.W.II), who worked on the terminal ballistics of armor plates. Another work from those times was by Taylor (1948). Their main results were summarized by Corbett et al. (1996) in terms of the work (W) which is needed to expand a hole of the projectile's radius (r_p), in a ductile plate of thickness H, made of a material with strength Y. The thickness of the plate in their analysis was the same as the diameter of the projectile. The two models start from somewhat different assumptions, concerning the state of the stress in the plate (see Corbett et al. (1996)), which result in the following expressions for this work:

$$W = 2\pi r_p^2 \cdot Y \cdot H = A \cdot 2Y \cdot H \quad \text{Bethe (1941)} \tag{10a}$$

$$W = 1.33\pi r_p^2 \cdot Y \cdot H = A \cdot 1.33Y \cdot H \quad \text{Taylor (1948)} \tag{10b}$$

where $A = \pi r_p^2$ is the area of the hole. This means that the effective stress, which acts on the projectile in this process, is equal to 2Y according to Bethe's model and to 1.33Y according to Taylor's model. The value σ_r=2Y is very close to the values we already found for $H/D = 1$, in both our simulations and the experiments cited above, for aluminum plates. In the next sections we describe simulation results for other projectile/target pairs. As the density of the plate does not enter into these equations our first goal was to check whether the effective stresses depend on plate density.

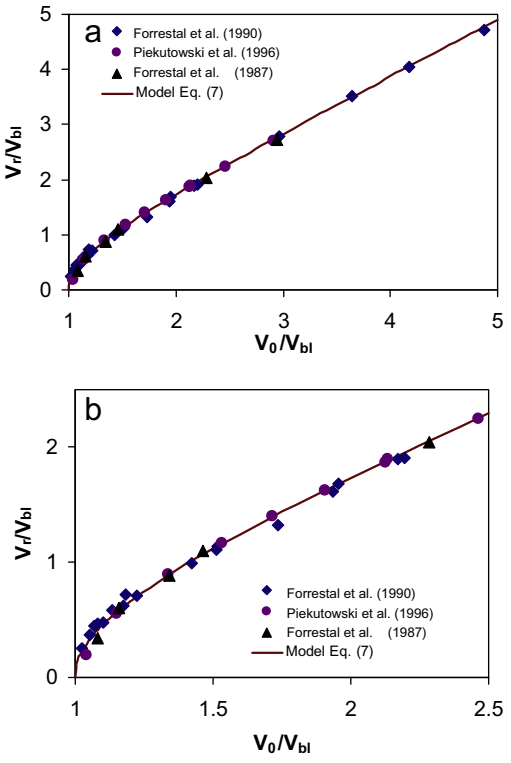

Fig. 7. Comparing the normalized results from Forrestal et al. (1990); Piekutowski et al. (1996); Forrestal et al. (1987) with Eq. (7): (a) showing all the results and (b) expanded view of the low velocity range.

5.2. Steel targets

The first set of simulations was performed with the same conical-nosed tungsten projectile impacting steel targets (with von-Mises strength of 0.4 GPa). As before, we used H = 8.3, 12.7, 50.8, 76.2 and 100 mm thick plates. In addition we simulated the deep penetration of this projectile into a semi-infinite target, at $V_0 = 800$ m/s, in order to obtain the corresponding value of R_t. The resulting constant deceleration, from this simulation, was $a = 4.76 \times 10^{-3}$ mm/(μs)^2. From Eq. (1) we get a value of $R_t = 2.254$ GPa, for this projectile/target combination. The residual velocities for the finite plates are given in Table 10 together with the inferred ballistic limit velocities for each simulation, as calculated by Eq. (4). Table 10 also lists the effective stresses (σ_r) for these plates, as calculated from Eq. (7). As is clearly seen, the value of σ_r for the 8.3mm plate ($H/D = 1$) is very close to 2Y, as for the aluminum plate, and as expected by Bethe's model, Eq. (10a). On the other hand, the values of σ_r for the thicker steel plates are higher than the corresponding values for the aluminum plates (see Table 3). This is probably due to the higher R_t value of the semi-infinite steel target (2.254 GPa) compared with that of the aluminum (1.894 GPa). The σ_r values for different material should approach their corresponding R_t value at large thicknesses. Thus, our conclusion from this set of simulations is that the density of the target does not play a very important role in determining its effective resisting stress.

Another simulation was performed for an 8.3 mm steel plate ($H/D = 1$), with strength of 0.8 GPa, perforated by the same conical-nosed projectile. An impact velocity of 300 m/s resulted in a residual velocity of $V_r = 184$ m/s. These values give $V_{bl} = 237$ m/s from Eq. (4), and $\sigma_r = 1.6$ GPa from Eq. (7), which is exactly twice the yield strength of the plate. Thus, our limited number of simulations

Table 10
Simulation results for conical-nosed tungsten projectiles perforating the 0.4 GPa steel plates.

H (mm)	V_0(m/s)	V_r (m/s)	V_{bl} (m/s)	σ_r (GPa)
8.3	200	109	167.7	0.805
	300	249	168.5	
12.7	300	204.3	220	0.93
	500	445.3	227	
50.8	800	566.5	564.8	1.49
76.2	800	352	718.4	1.6
100	900	301	848	1.7

support the analysis of Bethe (1941), namely, that σ_r=2Y for the special case of H/D = 1.

5.3. Ogive-nosed projectiles

In order to learn something about the influence of the projectile's nose shape on the ballistic limit velocities, and the effective stresses, we simulated an ogive-nosed tungsten projectiles, 8.3 mm in diameter, impacting the same aluminum plates (with a strength of 0.4 GPa), at different velocities. We used a short ogive (1.5CRH) in order to have a significantly different nose shape, compared to the conical. This projectile has a total length of 30 mm and an effective length of 25.9 mm. Table 11 lists the different values for the impact and residual velocities, together with the inferred ballistic limits and effective stresses, which were calculated as before. We also simulated the deep penetration of this ogive nosed projectile impacting a semi-infinite aluminum target (with strength of 0.4 GPa), at 800 m/s. The deceleration at deep penetration was 4.2×10^{-3} mm/μs^2 which, from Eq. (1), results in a value of $R_t = 2.01$ GPa for this projectile/target combination.

As for the other cases, the value of σ_r for the 8.3 mm plate (H/D = 1) is close to 2Y, for this ogive nosed projectile. For the thicker plates we obtained σ_r values which are higher than the corresponding values for the conical-nosed projectile, by 5–10% (see Table 3), probably because of the higher R_t value for this ogive nosed projectile. This may not seem a large difference but it certainly tells us that the nose shape has some relevance to σ_r for plates with $H/D \geqslant 1$.

5.4. Thin plates ($H/D < 1$)

In order to explore the limiting value of σ_r, for very thin plates, we performed several simulations for 0.4 GPa steel plates, with H=2, 4 and 8.3 mm perforated by the same conical-nosed tungsten projectiles. These are very thin plates which can bend easily and absorb more energy from the projectile by this bending as discussed by Woodward (1978). In order to check the effect of plate bending we performed these simulations also with aluminum projectiles. Table 12 summarizes the results of these simulations from which we can clearly see that for thin plates ($H/D < 1$) the values of σ_r/Y change quite appreciably with the H/D ratio. It is interesting to note that the simulation of the aluminum projectile perforating the 8.3 mm thick steel plate resulted in σ_r=0.8 GPa which is exactly 2Y, as for the tungsten projectile, and in line with Bethe's model.

Table 11
Simulation results for ogive-nosed tungsten projectiles perforating the 0.4 GPa aluminum plates.

H (mm)	V_0 (m/s)	V_r (m/s)	V_{bl} (m/s)	σ_r (GPa)
8.3	200	103	171.5	0.82
	300	248.6	167.9	
12.7	300	204	220	0.94
	500	448	222	
	800	767	227	
50.8	600	253	544	1.42
	800	583	548	
	1000	832	555	
76.2	800	375.8	706	1.57
100	900	328	838	1.69
	1100	708	841	

Table 12
Simulation results for tungsten and aluminum conical-nosed projectiles perforating thin steel plates.

Projectile	H (mm)	V_0 (m/s)	V_r (m/s)	V_{bl}(m/s)	σ_r (GPa)
Aluminum	2	200	101	173	0.52
	4	300	107	280.2	0.68
		400	284.5	281.2	
	8.3	500	241.6	437.8	0.8
Tungsten	2	200	188.2	67.7	0.54
	4	300	279.1	109.9	0.71
	8.3	200	109	167.7	0.8

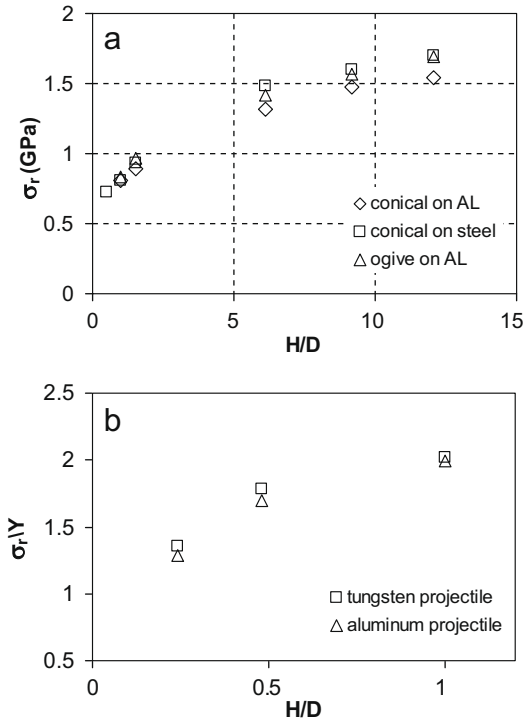

Fig. 8. Our simulation results for the change in σ_r with normalized target thickness: (a) tungsten projectiles perforating 0.4 GPa aluminum and steel targets and (b) thin steel targets perforated by conical-nosed tungsten and aluminum projectiles.

Finally, we show in Fig. 8 all our simulation results for σ_r as a function of H/D, for the conical and ogive nosed projectiles perforating aluminum and steel targets. Fig. 8a gives the results for plates with $H/D \geqslant 1$, while Fig. 8b shows the results for the thin steel targets ($H/D \leqslant 1$). One can clearly see in Fig. 8a that the effective stresses start from about σ_r=0.8 GPa (2Y), for H/D = 1, and increase asymptotically towards their respective R_t values. In Fig. 8b, for the thin plates, we see that the difference between the results for tungsten and aluminum projectiles is quite small, considering the large difference in their densities. We also note that the values for σ_r are decreasing very steeply for thinner plates. It would be very interesting to perform similar simulations for much thinner targets in order to find the transition from ductile hole enlargement to bending and dishing failure, as discussed by Woodward (1978). However these simulations are more difficult to perform and they are outside the scope of the present paper. An interesting point to note here is that our results for σ_r/Y as a function of H/D seem to extrapolate to a value near $\sigma_r/Y = 0.5$ for diminishing plate thickness. This is exactly the value which the model of Thomson (1955) predicts for the resisting stress in a very thin plate. In conclusion, our simulations show a strong dependence of σ_r on the thickness of the perforated plate, especially for thin plates with $H/D \leqslant 1$.

5.5. An example for our model's applicability

As a final demonstration for the usefulness of our approach we wish to analyze the data of Borvik et al. (2004) which we already

mentioned earlier. These experiments were recently simulated in (Borvik et al., 2009) and compared with the predictions from an analytical model which is based on the dynamic cavity expansion analysis. The agreement between experimental results for V_{bl} values and the model predictions is within 9–15%. We shall demonstrate here that our simple approach agrees with the data of (Borvik et al., 2004) to a much better extent. The flow stresses of the different plates, as given in Figs. 2 and 3 in (Borvik et al., 2009), are: $Y = 0.5$ GPa for the 15 mm plate, $Y = 0.45$ GPa for the 20 and 30 mm plates and $Y = 0.4$ GPa for the 25 mm plate. Considering the different H/D values for these plates we get from Fig. 8b the following values σ_r= 1.8Y, 2Y, 2.15Y and 2.3Y for the 15 mm, 20 mm, 25 mm and 30 mm plates, respectively. Thus: $\sigma_r = 0.9$ GPa for the 15 and 20 mm plates, $\sigma_r = 0.86$ GPa for the 25 mm plate and $\sigma_r = 1.035$ GPa for the 30 mm plate. Using these values in Eq. (7), together with the values of $\rho_p = 7.85$ g/cc and $L_{eff} = 78$ mm, we finally get the following values: $V_{bl} = 210$, 242.5, 265 and 318.5 m/s for the 15, 20, 25 and 30 mm plates, respectively. The experimental results from (Borvik et al., 2004) for V_{bl} are: $V_{bl} = 216.8 \pm 2.2,\ 249 \pm 3,\ 256.6 \pm 7$ and 309.7 ± 4.7 m/s for these plates, respectively. One can clearly see that our predictions are in excellent agreement with the experimental results, strongly enhancing the validity and usefulness of our approach.

6. Concluding remarks

We presented a large number of 2D numerical simulations of deep penetrations and plate perforations by sharp-nosed rigid projectiles. We focused our attention on the effects of the entrance phase on the resisting stress, which a short projectile experiences during its penetration into a semi-infinite target. We showed that the influence of this phase is dominant at ordnance velocity range (up to about 1.0 km/s) and that it diminishes only for penetration depths which are about four to six times the projectile diameter. For deeper penetrations we found that the force on the projectile is constant, as in (Rosenberg and Dekel, 2009) for rigid long rods. The second issue which we dealt with here is the perforation of ductile targets by sharp nosed projectiles and long rods. We followed the resisting stresses on these rigid sharp-nosed projectiles, with the 2D numerical simulations. We showed that these stresses are far from constant, due to the enhanced effect of the back free surface of the plate. However, as demonstrated here, the simple analysis of Recht and Ipson (1963) for the ballistic limit velocities, applies for a large range of plate thicknesses and impact velocities. Thus, a single normalized curve can be used for all sets of experiments in order to account for the residual velocity in terms of the impact and the ballistic limit velocities. The only difference between these sets is through the corresponding values of the ballistic limit velocity. We also defined an effective resisting stress (σ_r) which can be assigned to a given metallic plate which is perforated by a sharp nosed projectile. This effective stress determines the ballistic limit velocity of the given target/projectile pair and we showed that it depends on both the strength of the plate and on its normalized thickness (H/D). We conclude this paper by suggesting that the main theoretical challenge, in the field of plate perforation, is to account for the dependence of this effective resisting stress on both the compressive strength and thickness of the plate. Once these relations are worked out analytically, the prediction of V_{bl}, for any projectile/target combination, follows immediately through the equations we derived here.

References

Bethe, H.A., 1941. An attempt at a theory of armor penetration, Ordnance Laboratory Report, Frankford Arsenal, May 23.

Bishop, R.F., Hill, R., Mott, N.F., 1945. The theory of indentation and hardness. Proc. Roy. Soc. 57, 145.

Borvik, T., Langseth, M., Hopperstad, O.S., Malo, K.A., 2002. Perforation of 12 mm thick steel plates by 20 mm diameter projectiles with flat, hemispherical and conical noses Part I. Experimental study. Int. J. Impact Eng. 27, 19.

Borvik, T., Clausen, A.H., Hopperstad, O.S., Langseth, M., 2004. Perforation of AA5083-H116 aluminum plates by conical-nosed steel projectiles – experimental study. Int. J. Impact Eng. 30, 367.

Borvik, T., Forrestal, M.J., Hopperstad, O.S., Warren, T.L., Langseth, M., 2009. Perforation of AA5083-H116 aluminum plates with conical-nose steel projectiles – Calculations. Int. J. Impact Eng. 36, 426.

Chen, X.W., Li, X.L., Huang, F.L., Wu, H.J., Chen, Y.Z., 2008. Damping function in the penetration/perforation struck by rigid projectiles. Int. J. Impact Eng. 35, 1314.

Corbett, G.G., Reid, S.R., Johnson, W., 1996. Impact loading of plates and shells by free flying projectiles: a review. Int. J. Impact Eng. 18, 141.

Dehn, J., 1986. A unified theory of penetration, Technical Report BRL-TR-2770.

Dikshit, S.N., Sundararajan, G., 1992. The penetration of thick steel plates by ogive shaped projectiles-experiment and analysis. Int. J. Impact Eng. 12, 373.

Forrestal, M.J., Warren, T.L., 2009. Perforation equations for conical and ogival nose rigid projectiles into aluminum target plates. Int. J. Impact Eng. 36, 220.

Forrestal, M.J., Rosenberg, Z., Luk, V.K., Bless, S.J., 1987. Perforation of aluminum plates by conical-nosed projectiles. J. Appl. Mech. 54, 230.

Forrestal, M.J., Luk, V.K., Brar, N.S., 1990. Perforation of aluminum armor plates with conical-nose projectiles. Mech. Mater. 10, 97.

Forrestal, M.J., Brar, N.S., Luk, V.K., 1991. Penetration of strain hardening targets with rigid spherical-nose rods. J. Appl. Mech. 58, 7.

Forrestal, M.J., Frew, D.J., Hickerson, J.P., Rohwer, T.A., 2003. Penetration of concrete targets with deceleration time measurements. Int. J. Impact Eng. 28, 479.

Goodier, J.N., 1965. On the mechanics of indentation and cratering in solid targets of strain hardening metal by impact of hard and soft spheres. In: AIAA Proceedings of the Seventh Symposium on Hypervelocity Impact, vol. III, pp. 215–259.

Hermann, W., Jones, A.H., 1961. Survey of hypervelocity impact information. MIT Aeroelastic and Structure Research Laboratory, Report No. 99-1, September.

Piekutowski, A.J., Forrestal, M.J., Poormon, K.L., Warren, T.L., 1996. Perforation of aluminum plates with ogive nose steel rods at normal and oblique impacts. Int. J. Impact Eng. 18, 877.

Piekutowski, A.J., Forrestal, M.J., Poormon, K.L., Warren, T.L., 1999. Penetration of 6061-T6511 aluminum targets by ogive nosed steel projectiles with striking velocities between 0.5 and 3.0 km/s. Int. J. Impact Eng. 23, 723.

Recht, R.F., Ipson, T.W., 1963. Ballistic perforation dynamics. J. Appl. Mech. 30, 384.

Rosenberg, Z., Dekel, E., 2009. The penetration of rigid long rods-revisited. Int. J. Impact Eng. 36, 551.

Rosenberg, Z., Forrestal, M.J., 1988. Perforation of aluminum plates with conical-nosed rods-additional data and discussion. J. Appl. Mech. 55, 236.

Taylor, G.I., 1948. The formation and enlargement of a circular hole in a thin plastic plate. Quart. J. Mech. Appl. Math. 1, 103.

Thomson, W.T., 1955. An approximate theory of armor penetration. J. Appl. Phys. 26, 80.

Woodward, R.L., 1978. The penetration of metal targets by conical projectiles. Int. J. Mech. Sci. 20, 349.